

Porcupine Feeding Scars and Climatic Data Show Ecosystem Effects of the Solar Cycle

Ilya Klvana,^{1,*} Dominique Berteaux,^{1,†} and Bernard Cazelles^{2,‡}

1. Canada Research Chair in Conservation of Northern Ecosystems and Centre d'Études Nordiques, Université du Québec à Rimouski, 300 Allée des Ursulines, Rimouski, Québec, Canada, G5L 3A1;

2. Institut de Recherche pour le Développement, Géométrie des Espaces Organisés, Dynamiques Environnementales et Simulations, 93143 Bondy cedex, France; and Centre National de la Recherche Scientifique, Unité Mixte de Recherche 7625, École Normale Supérieure, 46 rue d'Ulm, 75230 Paris cedex 05, France

Submitted September 8, 2003; Accepted April 20, 2004;
Electronically published August 16, 2004

Online enhancements: appendixes, figures.

ABSTRACT: Using North American porcupine (*Erethizon dorsatum*) feeding scars on trees as an index of past porcupine abundance, we have found that porcupine populations have fluctuated regularly over the past 130 years in the Bas St. Laurent region of eastern Quebec, with superimposed periodicities of 11 and 22 years. Coherency and phase analyses showed that this porcupine population cycle has closely followed the 11- and 22-year solar activity cycles. Fluctuations in local precipitation and temperature were also cyclic and closely related to both the solar cycle and the porcupine cycle. Our results suggest that the solar cycle indirectly sets the rhythm of population fluctuations of the most abundant vertebrate herbivore in the ecosystem we studied. We hypothesize that the solar cycle has sufficiently important effects on the climate along the southern shore of the St. Lawrence estuary to locally influence terrestrial ecosystem functioning. This constitutes strong evidence for the possibility of a causal link between solar variability and terrestrial ecology at the decadal timescale and local spatial scale, which confirms results obtained at greater temporal and spatial scales.

Keywords: animal cycles, solar cycle, climatic oscillations, North American porcupine, *Erethizon dorsatum*, dendrochronology.

* E-mail: crazy_kayaker@hotmail.com.

† Corresponding author; e-mail: dominique_berteaux@uqar.qc.ca.

‡ E-mail: cazelles@wotan.ens.fr.

With the increasing impact of human activities on climate and ecosystems, it is of utmost importance to disentangle naturally occurring changes from human-induced changes. The clarification of the relative importance of variations in solar activity, volcanic activity, and anthropogenic sources in climate forcing is of particular concern (Mann et al. 1998; Crowley 2000). Although greenhouse gases have become the dominant force explaining climate change during the twentieth century, solar activity has probably played a major role in climate forcing during preindustrial times (Mann et al. 1998; Crowley 2000). Several studies have revealed that changes in solar activity on a timescale of centuries to millennia have had significant impacts on the climate of different regions (Verschuren et al. 2000; Bond et al. 2001; Hodell et al. 2001), with probably a cascading effect on human cultural development (Verschuren et al. 2000; Hodell et al. 2001). On the timescale of the 11-year and 22-year solar cycles, there is also growing evidence of a possible link between solar variability and climate, although this link remains somewhat unclear (Hoyt and Schatten 1997; Haigh 2000; Rind 2002).

Because one can expect solar-induced climatic oscillations to have an effect on ecosystem functioning, ecologists have considered the possibility that the 11-year solar cycle could play a role in driving, or at least synchronizing, the well-known decadal population cycle of many North American mammals (Elton 1924; Sinclair et al. 1993; Krebs et al. 2001). However, the “sunspot hypothesis” was rejected on several occasions (McLulich 1937; Elton and Nicholson 1942; Moran 1949, 1953a, 1953b; Royama 1992; Lindstrom et al. 1996).

Here we present independent evidence from a completely new system supporting the hypothesis of a link between the solar cycle, climate, and the cyclical nature of some animal populations in northern ecosystems. Using feeding scars left on trees by a locally dominant vertebrate herbivore, the North American porcupine (*Erethizon dorsatum*), we show that porcupine abundance has fluctuated periodically since 1868 in the Bas St. Laurent region of eastern Quebec. We demonstrate a strong relationship between this porcupine cycle, fluctuations in local precipi-

tation and temperature records, and the solar cycle. Our results suggest that the solar cycle can have sufficiently important impacts on the climate of certain areas to indirectly set the rhythm of animal population fluctuations. We believe this study constitutes strong evidence for the possibility of a causal link between solar variability and terrestrial ecology at the decadal timescale and local spatial scale.

Methods

Porcupine Feeding Scars

The North American porcupine is an arboreal rodent found over most of North America (Roze 1989). It is the dominant vertebrate herbivore (D. Berteaux, unpublished data) in our forested study system in the Lower St. Lawrence region of eastern Quebec, Canada (48°20'N, 68°50'W). Porcupine life history is characterized by high adult survival and low fecundity. Females usually attain sexually maturity at the age of 2.5 years and produce one young per year almost every year (Roze 1989). Porcupines can live up to 12 years of age (Earle and Kramm 1980). Limited data on porcupine population dynamics suggest that this species undergoes important population fluctuations, but no clear population cycle has been found until now (Spencer 1964; Payette 1987). The porcupine's summer diet is composed of leaves, buds, and fruits of deciduous trees and forbs. In winter, it is restricted to the inner bark of trees and conifer foliage (Roze 1989). The low nutritional quality of its winter diet leads to loss of body mass and deterioration of body condition and ultimately to increased mortality rates through starvation and predation (Sweitzer and Berger 1993).

Porcupines feeding on the inner bark of trees produce characteristic and easily recognizable oval feeding scars, often bearing visible teeth marks (Spencer 1964; Payette 1987). Because porcupines do not remove xylem tissue when feeding on bark, the year of scar formation can be determined by counting growth rings added since scar formation. We used coring to date porcupine feeding scars found on jack pine trunks (*Pinus banksiana*) at three sites (mean distance between sites = 9 km; total area sampled = 21 ha). We present a map of study sites in figure D1 in appendix D in the online edition of the *American Naturalist* and give technical details about scar sampling in appendix A in the online edition of the *American Naturalist*. All stands were located on dry, rocky hills within 1 km of the St. Lawrence estuary. We chose jack pine for sampling of scars for three reasons: first, its bark is highly used by porcupines; second, scars remain visible and well preserved for more than a century (see an example in fig. D2 in the online edition of the *American*

Naturalist); and third, jack pine growth rings are clearly visible, allowing accurate dating (we give technical details on scar dating in app. A and show a photograph of cores in fig. D3 in the online edition of the *American Naturalist*). A total of 501, 487, and 302 scars were dated on 357, 369, and 206 trees at sites 1, 2, and 3, respectively.

The frequency distribution of the number of feeding scars per year was computed for each site. This frequency distribution has been shown to be a good indicator of relative porcupine abundance (Spencer 1964). This is similar to the relationship between feeding scars on willow (*Salix* spp.) stems and vole (*Microtus agrestis* and *Clethrionomys glareolus*) abundance (Danell et al. 1981), between feeding scars on willow stems and lemming (*Lemmus sibiricus* and *Dicrostonyx groenlandicus*) abundance both in Eurasia and Arctic North America (Danell et al. 1999; Erlinge et al. 1999; Predavec et al. 2001), between dark stress marks in the rings of browsed white spruce and snowshoe hare abundance (Sinclair et al. 1993), and between trampling scars on roots and caribou (*Rangifer tarandus*) activity (Morneau and Payette 1998, 2000). Nonsystematic interviews with past and present residents and users of our study area also confirmed the close link between fluctuations in porcupine abundance and our scar data.

Our ongoing study of a tagged population of more than 100 porcupines 3 km east of stand 1 suggests that individual dispersal movements are short and that there is probably little exchange of individuals between our sites (D. Berteaux, unpublished data). The main predator of porcupines in the study area, the fisher (*Martes pennanti*), may, however, travel over long distances in short periods of time (Powell 1982). Therefore, our study sites cannot be considered as true replicates, and scar data from all three sites were pooled together for analysis. Separate analysis of scar data from each site was used only to verify that fluctuations were synchronous among sites (we graphically present data from each site, as well as the phase correspondence between sites, in fig. D4 in the online edition of the *American Naturalist*). Prior to pooling, data from each site was weighed according to sampling effort (weight used for a given site = mean number of scars per year at that site/mean number of scars per year for all sites). Given the varying length of the time series, the average number of scars per year for all sites was based on data from the three sites for the period 1944–2000, from sites 1 and 2 for 1906–1943, and only from site 1 for 1868–1905. All raw data on porcupine feeding scars can be downloaded from <http://wer.uqar.qc.ca/chairedb/porcupinecycle.xls>.

Solar Activity Data

We used reconstructed solar irradiance, as calculated by Lean et al. (1995), as an index of solar activity. Solar irradiance time series reflect variations in the sun's output of visible and ultraviolet light, x-rays, and cosmic rays (Foukal 1990; Hoyt and Schatten 1997; Storini and Sykora 1997; Mursula et al. 2001). Solar irradiance is more likely to be a biologically and climatically explicative measure of solar activity than the traditionally used sunspot number. However, we also performed analyses using the sunspot number, given its widespread use in the ecological literature. Sunspot data were obtained from the World Data Center for the Sunspot Index (2001). All solar activity data used in this study can be downloaded from <http://wer.uqar.qc.ca/chairedb/porcupinecycle.xls>.

Climatic Data

The climate of our study system is characterized by cold winters (mean January temperature = -12.0°C , 1971–2000) and mild summers (mean July temperature = 17.7°C , 1971–2000). Precipitation is relatively abundant and is distributed uniformly throughout the year (total annual precipitation = 1,005.3 mm, 1971–2000).

We obtained monthly temperature and precipitation records from the Meteorological Service of Canada (2000) for the two weather stations closest to our study sites. The Trois-Pistoles station ($48^{\circ}09'\text{N}$, $69^{\circ}07'\text{W}$; mean distance from study sites = 25 km) provided data for 1951–2000. The Pointe-au-Père station ($48^{\circ}30'\text{N}$, $68^{\circ}29'\text{W}$; mean distance from study sites = 35 km) provided data for 1877–1951. Because there was no station in the vicinity of our study sites with a complete record for the entire period, the data from the two stations were spliced together (Pointe-au-Père, 1877–1951; Trois-Pistoles, 1952–2000) to form a continuous 1877–2000 time series. Mean temperature and total precipitation were calculated from the monthly data for the following four periods of each year:

November to April inclusive. Hereafter, we will refer to this as winter, the most critical period for porcupines because first, vegetation is dormant in our study area, restricting the porcupine's diet to low-quality tree bark and conifer foliage; second, most precipitation (70.5%) falls in the form of snow, greatly increasing the energetic cost of movement, as has been shown for other mammalian herbivores (Parker et al. 1984); and third, cold temperatures greatly increase the costs of thermoregulation. In addition to mean winter temperature and total precipitation, we also calculated total snowfall. Although snow penetrability may be more relevant to porcupine winter ecology, only snowfall data was available.

May to October inclusive. Hereafter, we will refer to this as summer, the period during which porcupines gain mass while feeding on leaves, buds, and fruits of deciduous trees and forbs (Roze 1989).

May and June. Hereafter, we will refer to this as spring, the period during which climate can be expected to have the greatest influence on the survival of newborn porcupines, most of them being born in mid-May in our study area (Roze 1989).

Winter and summer periods combined. We combined these periods over the entire year. This includes the period from November to October.

In addition to these climatic variables, we used the North Atlantic Oscillation (NAO) index as a measure of global climatic variations, both for annual and winter periods, as defined by Hurrell (1995). The NAO index data were obtained from the Climatic Research Unit (2001). All climate data used in this study can be downloaded from <http://wer.uqar.qc.ca/chairedb/porcupinecycle.xls>.

Statistical Methods

Fourier analysis has traditionally been used to analyze relationships between oscillating time series. Fourier analysis decomposes time series into their different periodic components, and these periodic components can then be compared from one series to the next. This method was initially developed for the analysis of physical phenomena but is not always appropriate when dealing with complex biological and climatic time series (Chatfield 1989) because it cannot take into account the often observed changes in the periodic behavior of such series (i.e., their lack of stationarity and homogeneity). We therefore used wavelet analysis (B. Cazelles et al., unpublished manuscript; Mallat 1998; Torrence and Compo 1998), which is well suited to explore local variations in frequency as time progresses. Wavelet analysis quantifies the temporal evolution of time series with different rhythmic components by performing the so-called time-frequency analysis of the signal. In addition to extracting the information on the different periodic components of a time series (which is similar to Fourier analysis), wavelet analysis thus indicates the evolution through time of these periodic components. Wavelet decomposition has recently been used with success in ecology (Bradshaw and Spies 1992; Dale and Mah 1998; Grenfell et al. 2001). It is particularly well adapted in the context of our study because it allowed us to determine whether the statistical association between two oscillating phenomena remained constant throughout time. We reasoned that a statistical association that is constant through time is much more indicative (although not demonstrative) of cause-effect relationships than a statistical association for which constancy through time has not been demonstrated.

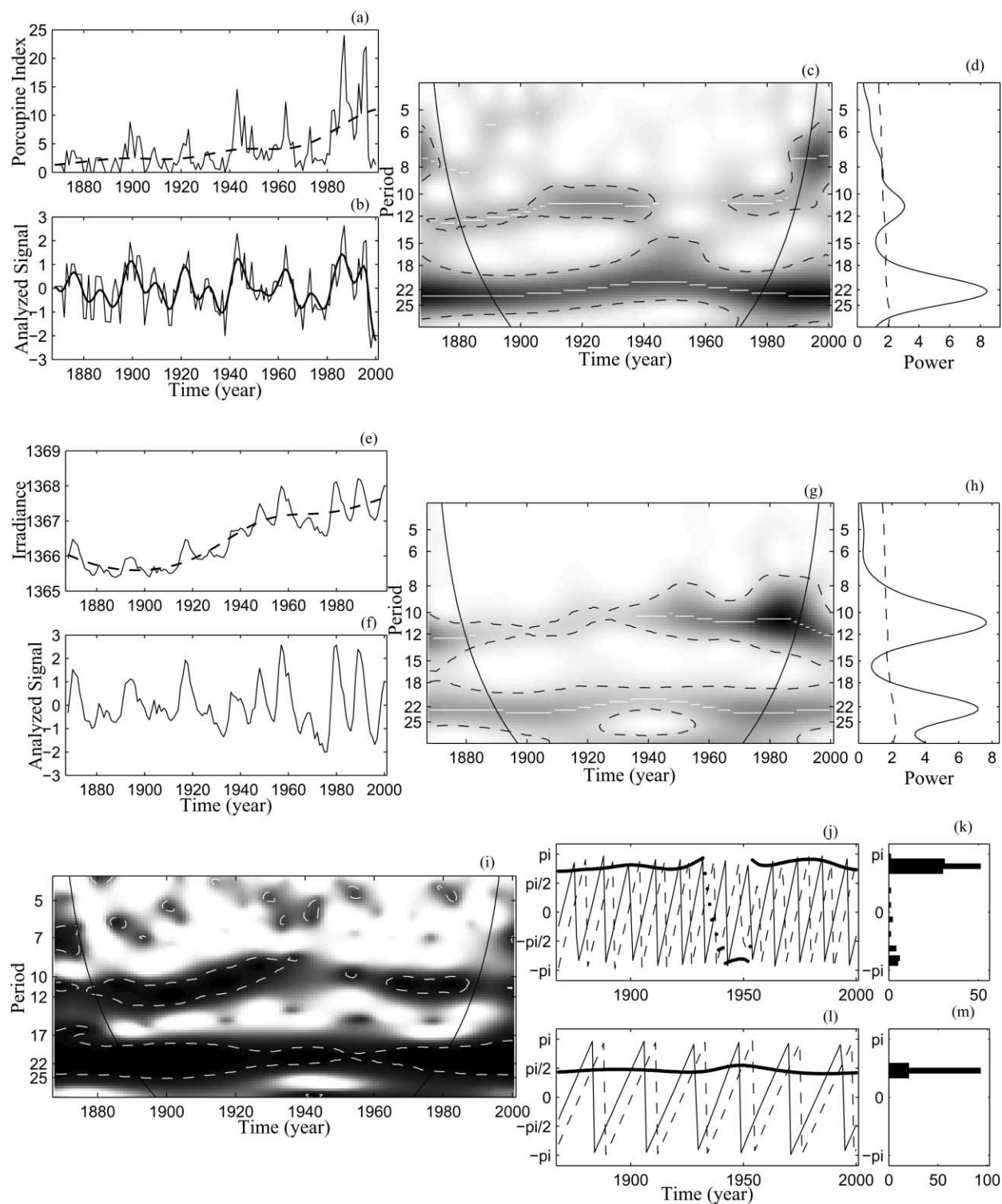


Figure 1: Wavelet analysis of porcupine abundance index and solar irradiance. *a*, Porcupine abundance index (*solid line*) calculated as the pooled frequency distribution of porcupine feeding scars from three sites in eastern Quebec, Canada. The dashed line shows high-period (>50 years) oscillating components. *b*, Analyzed time series (*thin line*) obtained by square root transformation of *a*, followed by detrending through the subtraction of high-period oscillating components. To underline the periodic components in the data, a smoothed series, obtained using Singular Spectrum Analysis (Vautard et al. 1992), is also shown (*bold line*); this last series was not used in the analysis. *c*, Local wavelet power spectrum (i.e., scalogram)

We present details about the wavelet analysis methodology in appendix B in the online edition of the *American Naturalist* (for a good introduction to wavelet time series analysis, see also box 1 in Grenfell et al. 2001).

Before wavelet analyses, all series were square root transformed in order to dampen extremes in variability. In addition, all oscillating components with a period greater than 50 years were estimated using a high-pass Gaussian filter (see, e.g., Park and Gambéroni 1995), and series were detrended by subtracting these oscillating components.

Results

Porcupine Feeding Scars and Solar Activity

Wavelet analysis revealed the presence of significant 11- and 22-year periodicities in the porcupine scar data (fig. 1*d*). Both cycles were present throughout the entire 133-year time series, except for a short loss of power in the 11-year cycle from 1944 to 1967 (fig. 1*c*). These 11- and 22-year periodicities mirror almost exactly the well-known 11- and 22-year solar cycle, as shown here by wavelet analysis of solar irradiance data for the same 1868–2000 time period (fig. 1*g*, 1*h*).

This striking similarity was supported by the strong and almost continuous coherence between the porcupine scar data and solar irradiance around those same 11- and 22-year periodicities (fig. 1*i*). The extraction of the 10–12-year (fig. 1*j*, 1*k*) and 21–23-year (fig. 1*l*, 1*m*) periodic components from both time series revealed that the phase difference between the two series was almost constant throughout time for both periodicities, indicating that the porcupine and solar cycles were very closely associated to each other, at least statistically. In the case of the 10–12-year cycle, the phase difference varied between $3/4\pi$ and π (fig. 1*k*), which corresponds approximately to a 5-year time lag between the porcupine cycle and the solar cycle (one cycle = $2\pi = 11$ years). As for the 21–23-year cycle, the phase difference between the two series was almost perfectly constant and only slightly less than $\pi/2$ (fig. 1*m*), corresponding again approximately to a 5-year time lag between the porcupine cycle and the solar cycle (one

cycle = $2\pi = 22$ years). The statistical association between solar irradiance and the porcupine cycle is also highly significant when the sunspot number is used as an index of solar activity (fig. D5*j*–D5*m* in the online edition of the *American Naturalist*), despite the fact that the 22-year cycle is completely hidden by the 11-year cycle in the sunspot index (fig. D5*g*, D5*h*).

Climatic Data

In an effort to understand the striking relationship between the porcupine cycle and the solar cycle, wavelet analysis was also applied to local weather data. Out of the 11 climatic variables analyzed (total annual precipitation, total winter precipitation, snowfall, total spring precipitation, total summer precipitation, mean annual temperature, mean winter temperature, mean spring temperature, mean summer temperature, winter NAO, and annual NAO), three displayed highly significant periodicities at the 11- and/or 22-year periods: spring temperature, winter precipitation, and snowfall.

Spring temperature displayed a significant and almost continuous 22-year periodicity (fig. 2*c*, 2*d*), which induced a high and continuous coherence between solar irradiance and spring temperature (fig. 3*a*) and between spring temperature and porcupine scars (fig. 3*f*) at the 22-year periodicity. In addition, phase analysis showed strong phase locking between these three series at the 22-year periodicity (fig. 3*d*, 3*e*, 3*i*, 3*j*). As expected by the absence of 11-year periodicity in the spring temperature data, there was a poor phase locking between spring temperature and solar irradiance (fig. 3*b*, 3*c*) and between spring temperature and porcupine scars (fig. 3*g*, 3*h*) at the 11-year periodicity.

Both the 11- and 22-year periodicities were present in the winter precipitation series (fig. 2*h*), with the 22-year cycle displaying greater continuity than the 11-year cycle (fig. 2*g*). Coherence with solar irradiance (fig. 4*a*) and with porcupine abundance (fig. 4*f*) was relatively continuous, and the phase difference between series remained relatively constant at both the 11- (fig. 4*b*, 4*c*, 4*g*, 4*h*) and 22-year (fig. 4*d*, 4*e*, 4*i*, 4*j*) periodicities. Only the 22-year cycle was present in the snowfall series (fig. 2*k*, 2*l*). This periodicity

of *b*. Low power values are represented in white and high power values in black. The black dashed lines show the $\alpha = 5\%$ significance level computed based on 500 bootstrapped series. The white lines indicate the crests of the oscillations on the scalogram. The cone of influence, which indicates the region not influenced by edge effects, is also shown. *d*, Global wavelet power spectrum (similar to the classical Fourier spectrum) of *b*. The dashed line shows the $\alpha = 5\%$ significance level computed based on 500 bootstrapped series. *e*, Reconstructed total solar irradiance, as defined by Lean et al. (1995). *f*, Data presented in *e* after square root transformation and detrending, as in *b*. *g*, Local wavelet power spectrum of *f*. *h*, Global wavelet power spectrum of *f*. *i*, Coherence between solar irradiance and porcupine abundance index; interpretation similar to scalograms *c* and *g*. *j*, Phase time series of solar irradiance (*thin solid line*) and porcupine abundance index (*dashed line*) computed in the 10–12-year periodic band. The bold line displays the phase difference evolution. *k*, Distribution of phase differences; normalized entropy of the distribution = 0.49, $P < .002$ based on 500 bootstrapped series. *l*, Same as *j* but computed in the 21–23 periodic band. *m*, Distribution of phase differences; normalized entropy of the distribution = 0.74, $P = .002$ based on 500 bootstrapped series.

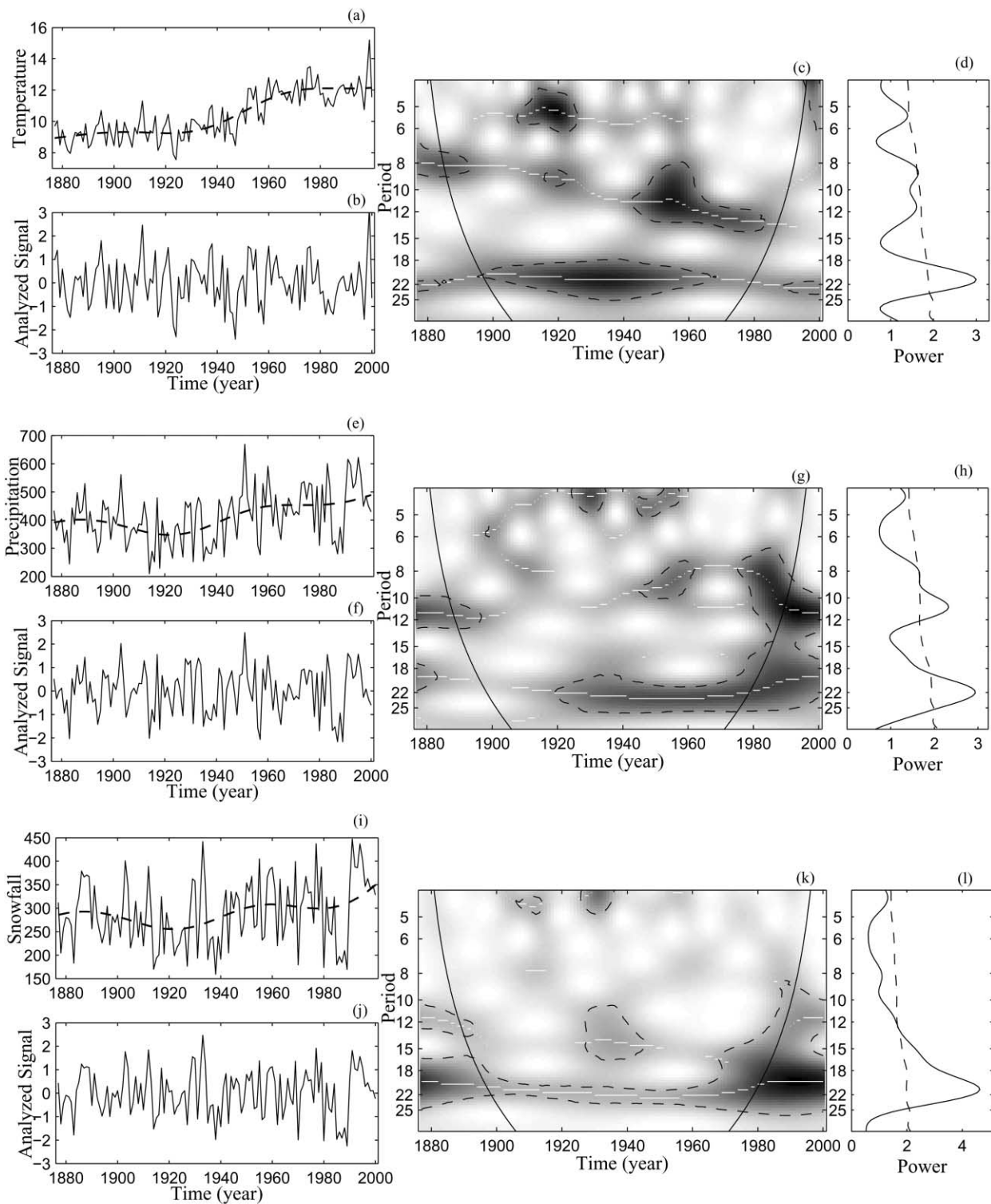


Figure 2: Wavelet analysis of climatic variables. *a*, Mean spring (May and June) temperature. The dashed line shows high-period (>50 years) oscillating components. *b*, Analyzed time series (*thin line*) obtained by square root transformation of *a*, followed by detrending through the subtraction of high-period oscillating components. *c*, Local wavelet power spectrum (i.e., scalogram) of *b*. Low power values are represented in white and high

led to a strong coherence and phase locking of snowfall with both solar irradiance (fig. 5a, 5d, 5e) and porcupine scars (fig. 5f, 5i, 5j) at the 22-year periodicity.

We show wavelet analyses performed on winter NAO in figure D6 in the online edition of the *American Naturalist* to present an example of a climatic variable that showed no continuous periodicity during the study period (fig. D6g, D6h). This absence of continuous periodicity led to an absence of significant coherence (fig. D6i) and phase locking (fig. D6j–D6m) between NAO and porcupine abundance.

Discussion

A Link between the Solar Cycle, Local Climate, and Porcupine Abundance

Our results provide several pieces of evidence for a strong relationship between the solar cycle and fluctuations in porcupine abundance. First, periodic components of 11 and 22 years were found in both solar irradiance and porcupine scar data. Second, we observed throughout our entire 1868–2000 time series a virtually constant phase relation between solar irradiance and porcupine scar data. Third, winter precipitation (mostly in the form of snow) and spring temperature were closely related to both solar irradiance and porcupine abundance and are thus candidate variables for a causal link between the solar and porcupine cycles. Our correlations do not demonstrate cause-effect relationships but represent strong support for the general hypothesis of a causal link between the solar cycle, local climate, and terrestrial ecology. Below we detail the set of specific hypotheses generated by our results.

The link between the solar cycle and local climate observed in our study system is relatively localized. For example, precipitation data from more distant weather stations (Quebec City, 250 km southwest of our study area; Cap Madeleine, 300 km east of our study area; Magdalen Islands, 600 km east of our study area) did not display the same regular 11-year and 22-year cycles. This is similar to the localized correlations that Perry (1994) found between precipitation fluctuations and the solar cycle in certain regions of the United States. Perry (1994) proposed that this pattern is a result of solar energy being stored in ocean water and transported by currents to certain regions where it is released, affecting regional climate. We suggest

that a similar hypothesis may very well apply to our study system because waters of the adjacent St. Lawrence estuary are known to warm up substantially during the summer from solar radiation (White and Johns 1997). Although solar irradiance varies by only about 0.1% from a solar minimum to a maximum (Haigh 2000), storage of this energy over one or several summers of high solar activity and over the whole St. Lawrence estuary, combined with its localized release in winter, could serve as an amplification mechanism allowing local climate to strongly respond to variations in solar activity. This would be in agreement with White et al. (1997), who found that excess heat in years of high solar activity is stored in the upper 100 m of the ocean and is eventually released to the atmosphere and not to the deep ocean. This hypothesis is clearly testable, although at present water temperature records for the St. Lawrence estuary are not sufficiently long. We present in appendix C in the online edition of the *American Naturalist* a succinct review of the literature on the effects of solar variability on the earth's climate in order to bring to ecologists the recent developments made in this field of research.

The mechanisms underlying the link between local climate and porcupine population dynamics also remain to be understood, although they appear more straightforward and easier to test. Our results strongly suggest that winter precipitation plays a key role in the population dynamics of porcupines. This hypothesis is in agreement with our present knowledge of porcupine biology. First, because of the short limbs of porcupines, winter precipitation greatly reduces individuals' mobility and access to food (Roze 1989). Second, porcupine mortality in our study area is greatest during winter, with individuals frequently dying from starvation (D. Berteaux, unpublished data; see also Roze 1989; Sweitzer and Berger 1993 for similar results in other porcupine study systems). Third, it is likely that stressful winter conditions negatively impact porcupine reproductive success, as is the case with other mammalian herbivores (Post et al. 1997; Forchhammer et al. 2001; Weladji and Holand 2003). The hypothesis that winter climate affects birth and death rates of porcupines is currently field tested in our study system. Our results also generate the hypothesis that spring temperature could affect the population dynamics of porcupines. This hypothesis echoes results from Langvatn et al. (1996) and Loison and Langvatn (1998), suggesting that spring temperature

power values in black. The black dashed lines show the $\alpha = 5\%$ significance level computed based on 500 bootstrapped series. The white lines indicate the crests of the oscillations on the scalogram. The cone of influence, which indicates the region not influenced by edge effects, is also shown. *d*, Global wavelet power spectrum (similar to the classical Fourier spectrum) of *b*. The dashed line shows the $\alpha = 5\%$ significance level computed based on 500 bootstrapped series. *e–h*, Same as *a–d* but for total winter precipitation (November to April, inclusive). *i–l*, Same as *a–d* but for total annual snowfall.

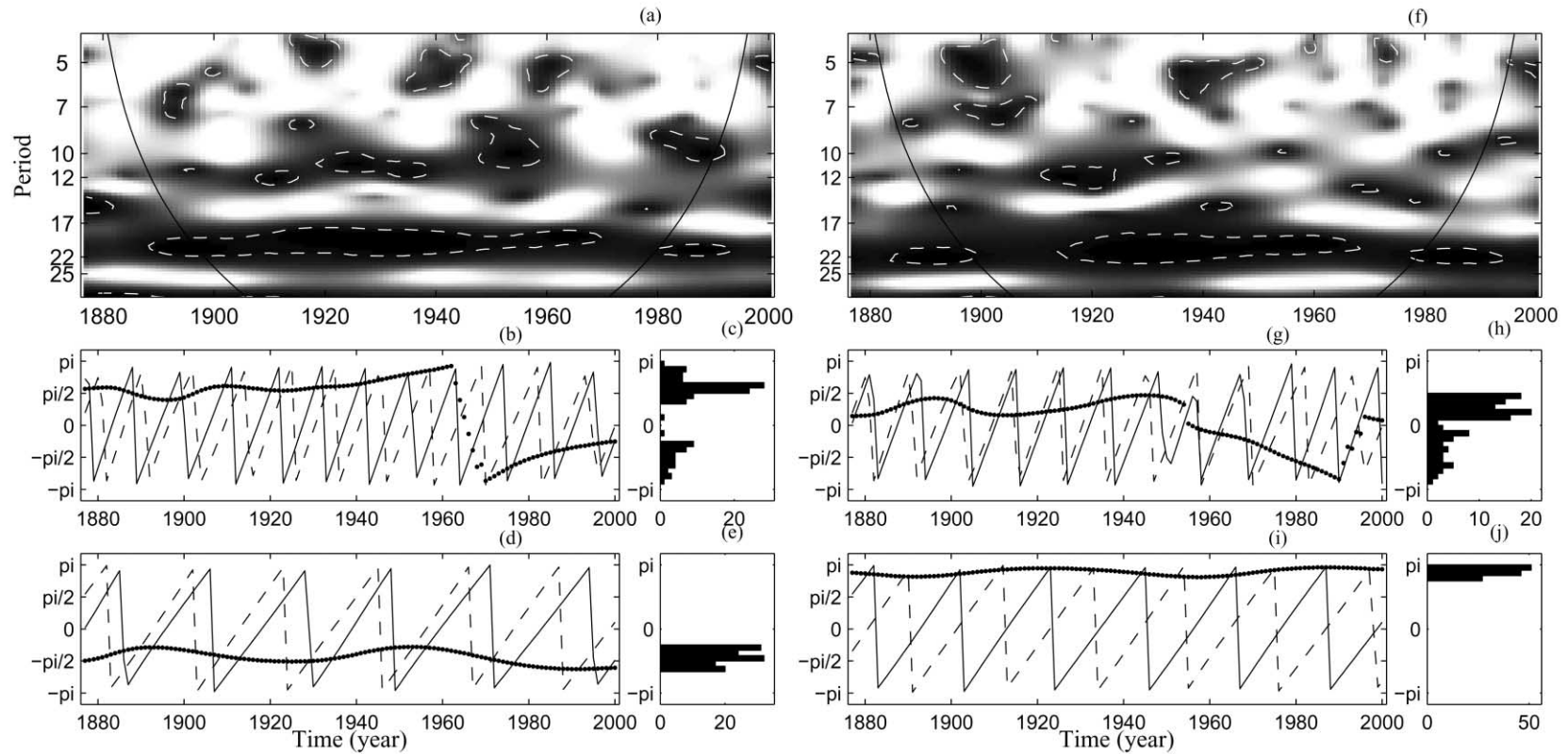


Figure 3: Coherence and phase analysis of mean spring temperature in relation to solar irradiance and porcupine abundance index. *a*, Coherence between solar irradiance and mean spring temperature. Low power values are represented in white and high power values in black. The white dashed lines show the $\alpha = 5\%$ significance level computed based on 500 bootstrapped series. The cone of influence, which indicates the region not influenced by edge effects, is also shown. *b*, Phase time series of solar irradiance (*thin solid line*) and spring temperature (*dashed line*) computed in the 10–12-year periodic band. The bold line displays the phase difference evolution. *c*, Distribution of phase differences; normalized entropy of the distribution = 0.22, $P > .1$ based on 500 bootstrapped series. *d*, Same as *b* but computed in the 21–23 periodic band. *e*, Distribution of phase differences; normalized entropy of the distribution = 0.50, $P = .04$ based on 500 bootstrapped series. *f*, Coherence between spring temperature and porcupine abundance index. *g*, Phase time series of spring temperature (*thin solid line*) and porcupine abundance index (*dashed line*) computed in the 10–12-year periodic band. The bold line displays the phase difference evolution. *h*, Distribution of phase differences; normalized entropy of the distribution = 0.40, $P = .014$ based on 500 bootstrapped series. *i*, Same as *g* but computed in the 21–23 periodic band. *j*, Distribution of phase differences; normalized entropy of the distribution = 0.66, $P = .016$ based on 500 bootstrapped series.

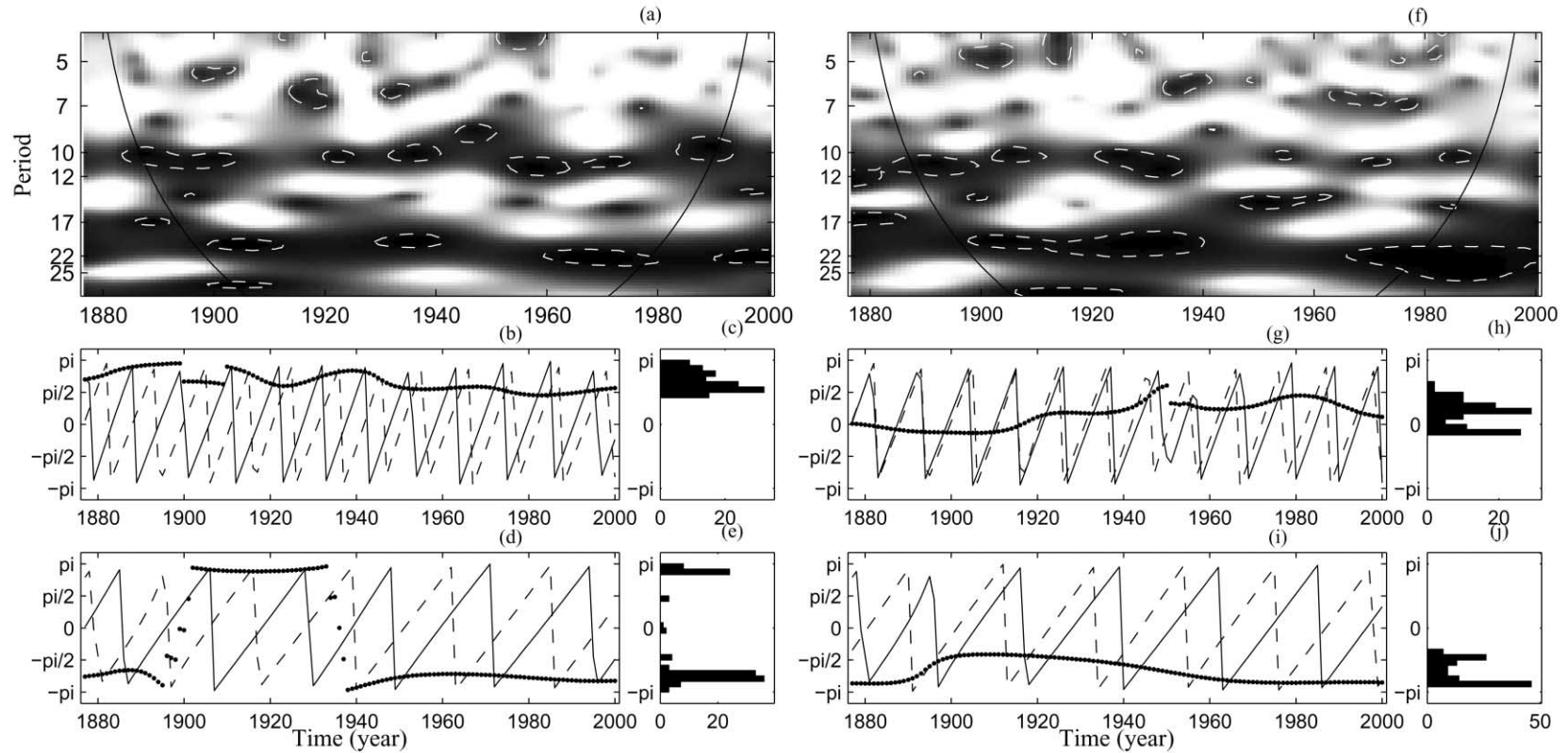


Figure 4: Coherence and phase analysis of total winter precipitation in relation to solar irradiance and porcupine abundance index. All symbols and values are as in figure 3. Normalized entropy of the distribution in $c = 0.41$, $P > .014$. Normalized entropy of the distribution in $e = 0.41$, $P > .1$. Normalized entropy of the distribution in $h = 0.36$, $P = .028$. Normalized entropy of the distribution in $j = 0.45$, $P > .1$.

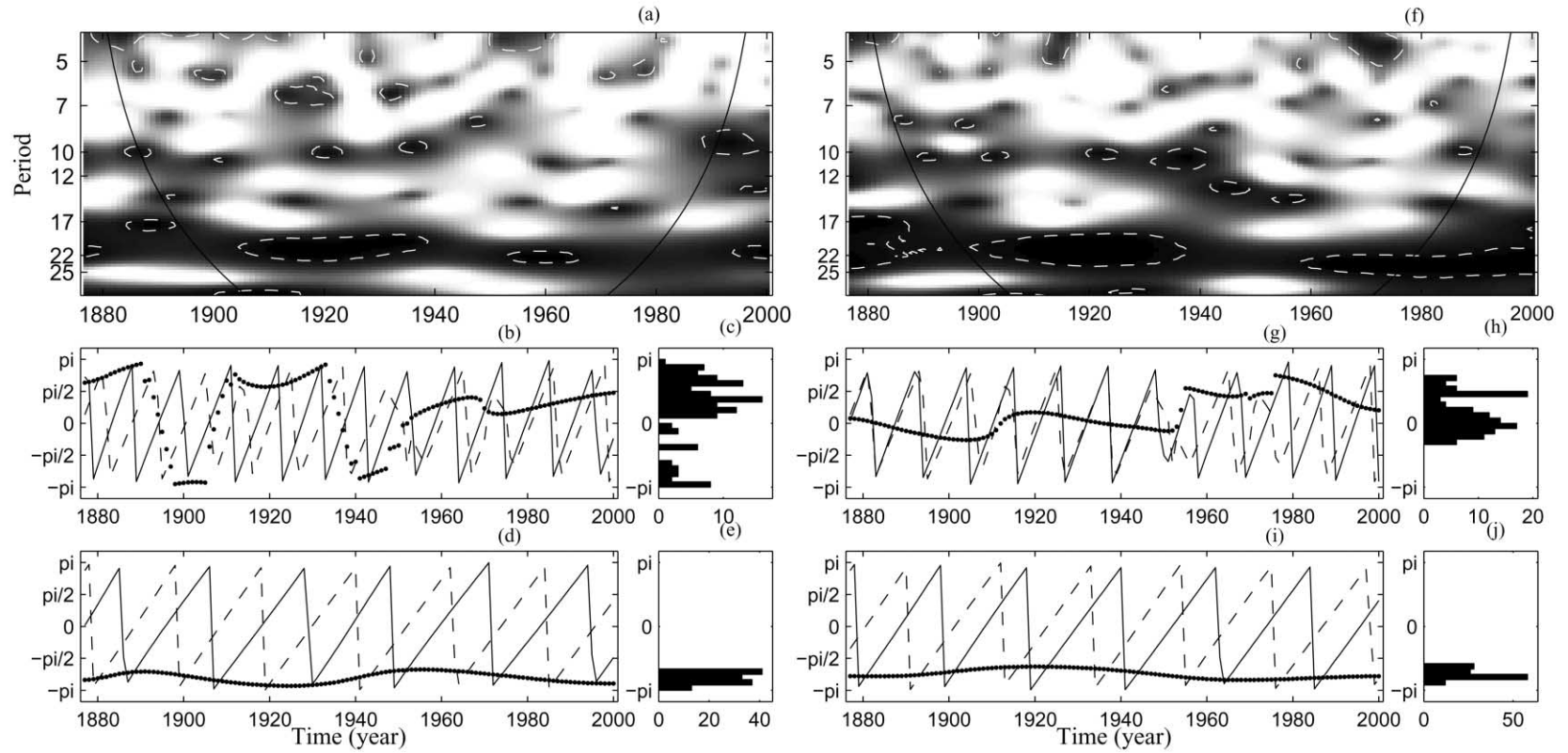


Figure 5: Coherence and phase analysis of total annual snowfall in relation to solar irradiance and porcupine abundance index. All symbols and values as in figure 3. Normalized entropy of the distribution in $c = 0.13$, $P > .1$. Normalized entropy of the distribution in $e = 0.58$, $P = .034$. Normalized entropy of the distribution in $h = 0.24$, $P > .1$. Normalized entropy of the distribution in $j = 0.60$, $P = .026$.

can have an important impact on the population dynamics of mammalian herbivores through its impact on forage quality and survival of juveniles.

Whereas research on other mammalian herbivores suggests that climatic variations do have the potential to induce population fluctuations through persistent cohort effects (Saether 1997; Post and Stenseth 1999), it would probably be naive to generate the simple hypothesis that the solar-induced climate cycle causes the porcupine population cycle (Stenseth et al. 2002). Rather, we hypothesize that delayed density-dependent factors alone may be sufficient to generate porcupine population fluctuations but that density-independent climatic factors may act as environmental pacemakers giving the porcupine cycle its observed periodicity. These environmental pacemakers would act through their recurrent perturbing influence on survival and reproductive success of individuals. This is analogous to the hypothesis stating that environmental variation generates spatial synchrony among populations over large geographical areas (Grenfell et al. 1998; Myers 1998; Bjørnstad et al. 1999; Hudson and Cattadori 1999; Stenseth et al. 1999; Cazelles and Boudjema 2001; Cazelles et al. 2003) and in a variety of taxa (mammals, Ranta et al. 1997*a*; birds, Cattadori et al. 2000; insects, Liebhold and Kamata 2000; reptiles, Chaloupka 2001).

Previous data on porcupine population fluctuations in other locations, although very scarce, support the idea that this species undergoes fluctuations in abundance but that these are not necessarily periodic. Keith and Cary (1991) reported a fivefold difference between extremes in porcupine abundance based on 11 years of capture data in Alberta, but their time series was too short to infer anything about the periodicity in population fluctuations. Spencer (1964) obtained 80 years of porcupine scar data in Colorado, and although he identified three peaks in porcupine abundance, these did not seem regularly spaced and were related neither to our data nor to the solar cycle. Payette (1987) used porcupine feeding scars as an indicator of past porcupine presence along the Hudson Bay coast of Quebec but found no periodicity in his results. It therefore appears that the periodicity of porcupine fluctuations found in our study system is not widespread but may exist only in certain locations in which there are strong climatic oscillations. Dendrochronological studies performed in ecosystems under various climatic regimes would allow testing of this hypothesis.

Population Cycles and the Solar Cycle Hypothesis

It is now well established that global climatic oscillations, such as the NAO and El Niño–Southern Oscillation (ENSO), can affect not only the population dynamics of mammalian herbivores (Post et al. 1997; Lima et al. 1999;

Forchhammer et al. 2001) but also entire ecosystems (Jakšic 2001; Ottersen et al. 2001; Blenckner and Hillebrand 2002; Stenseth et al. 2002). Similarly, we hypothesize that the climate of certain regions (such as the area surrounding the St. Lawrence estuary) responds particularly well to decadal variations in solar activity and that this solar-induced climatic oscillation has cascading effects on entire ecosystems. Our finding of a link between the solar cycle and fluctuations in the abundance of the dominant mammalian herbivore in a forest ecosystem may therefore be just an example of a more global phenomenon.

At present, however, we know of only two examples of a solar-induced climatic oscillation acting as an environmental pacemaker to animal population dynamics. Using browsing stress marks produced in the tree rings of white spruce (*Picea glauca*) by snowshoe hare (*Lepus americanus*), Sinclair et al. (1993) reconstructed past fluctuations in hare abundance at Kluane, Yukon. Analysis of this tree ring data revealed that during periods when the amplitude of the 11-year sunspot cycle was particularly high, hare abundance did cycle in phase with the sunspot cycle, although it came out of phase at other times. On the basis of this evidence, as well as climatic data linked with the sunspot cycle, they suggested that the snowshoe hare cycle “is modulated indirectly by solar activity through an amplified climate cycle that affects the whole boreal forest ecosystem” (Sinclair et al. 1993, p. 195). Ranta et al. (1997*b*) criticized the validity of this hypothesis and argued that hare cycles in Finland are not synchronized with those in North America and that the level of synchrony between local hare populations decreases with increasing distance both in Finland and Canada (Smith 1983). This, according to them, was contrary to what one would expect if an external factor was “setting the beat” of the hare cycle. Lindstrom et al. (1996) also rejected the possibility of a solar cycle–climate–hare–lynx causal relationship based on a time series analysis of the famous 1821–1934 Mackenzie River lynx fur return time series and sunspot data for the same period. Sinclair and Gosline (1997) reanalyzed the data used by Ranta et al. (1997*b*) and found that although local hare populations are not always in phase across Canada, they do come into phase during the peak years, suggesting the influence of an external synchronizer such as weather acting on a continental scale. They maintained their hypothesis that solar activity, when it is particularly strong, acts indirectly as the synchronizer of the hare cycle through its effect on climate. They specified that because weather systems have different phase relations with solar activity in different areas of the globe, we can expect that solar-hare phase relations will also differ (Sinclair and Gosline 1997).

The sunspot hypothesis was also put forth to explain synchrony and periodicity of insect outbreaks, although

again the empirical evidence was not strong enough to conclude a strong relationship (Myers 1998; Ruohomäki et al. 2000). Our results thus appear unique in that they are the first example of a population cycle that follows both the solar cycle and local climate fluctuations with such regularity and consistency over an extended period of time (130 years).

As shown above, the possibility of a link between the solar cycle, climate, and animal cycles has generated a vigorous debate (MacLulich 1937; Elton and Nicholson 1942; Moran 1949, 1953*a*, 1953*b*; Royama 1992; Lindstrom et al. 1996) and is still active 80 years after it was first put forth by Elton (1924). This underscores how difficult it is to either accept or reject the hypothesis of a solar cycle, population dynamics link. This difficulty partly stems from the fact that very few long time series of animal population fluctuations are available for analysis. When these ecological time series exist, their analysis is often complicated by their lack of linearity and stationarity (Cazelles and Stone 2003). In addition, even if empirical correlations are found, testing them with manipulative experiments is very difficult. Finally, the influence of the solar cycle seems discontinuous in time (it can disappear or even reverse phases during periods of low-amplitude solar cycles) and space (it can have different effects in different geographical areas; Hoyt and Schatten 1997), which complicates generalizations to be drawn from individual studies.

The solar cycle hypothesis raises questions about the approach that should be used to test it. Holling and Allen (2002) recently summarized what we think is the best avenue to progress in such complex, multisystem, and multiscale science. They proposed that to distinguish credible from incredible patterns in nature, a cycle of inquiry (called “adaptive inference”) is the most likely to lead to progress. In this cycle, no unambiguous test can distinguish among alternative hypotheses. Only a suite of tests of different kinds can do so, producing a body of evidence in support of one line of argument and not others. This contrasts with strong inference (Platt 1964), which is based on hypothesis falsification and where the main objective is to avoid Type I error. Research on both the multiyear population cycles of northern mammals and the effects of solar variability on climate and ecosystems is likely to benefit from the use of adaptive inference in addition to strong inference.

Acknowledgments

We thank C. Daguerre and P. Morin for field assistance and Parc National du Bic for providing facilities. P. Morin and two anonymous reviewers provided many helpful comments on the manuscript. I.K. was supported by an M.S. scholarship from the Natural Sciences and Engi-

neering Research Council of Canada (NSERC). B.C. was partially supported by the French Ministry of Ecology and Sustainable Resources, through grants Quantification des Risques d'Émergence d'Épidémies à Choléra dans le Bassin Méditerranéen en Relation avec le Changement Climatique and Modélisation des Arboviroses Tropicales Émergentes Climato-dépendantes of the program Gestion et Impacts du Changement Climatique. Research was funded by grants to D.B. from the NSERC, the Fonds de Recherche sur la Nature et les Technologies du Québec, and the Canada Research Chair program.

Literature Cited

- Bjørnstad, O. N., R. A. Ims, and X. Lambin. 1999. Spatial population dynamics: analyzing patterns and processes of population synchronicity. *Trends in Ecology & Evolution* 14:427–432.
- Blenckner, T., and H. Hillebrand. 2002. North Atlantic Oscillation signatures in aquatic and terrestrial ecosystems: a meta-analysis. *Global Change Biology* 8:203–212.
- Bond, G., B. Kromer, J. Beer, R. Muscheler, M. N. Evans, W. Showers, S. Hoffman, R. Lotti-Bond, I. Hajdas, and G. Bonani. 2001. Persistent solar influence on North Atlantic climate during the Holocene. *Science* 294:2130–2136.
- Bradshaw, G. A., and T. A. Spies. 1992. Characterizing canopy gap structure in forest using wavelet analysis. *Journal of Ecology* 80:205–215.
- Cattadori, I. M., S. Merler, and P. J. Hudson. 2000. Searching for mechanisms of synchrony in spatially structured gamebird populations. *Journal of Animal Ecology* 69: 620–638.
- Cazelles, B., and G. Boudjema. 2001. The Moran effect and phase synchronization in complex spatial community dynamics. *American Naturalist* 157:670–676.
- Cazelles, B., and L. Stone. 2003. Detection of imperfect population synchrony in an uncertain world. *Journal of Animal Ecology* 72:953–968.
- Cazelles, B., G. Boudjema, and L. Stone. 2003. Chaos synchrony induced by environmental perturbations in chaotic populations. Pages 262–269 in V. Capasso, ed. *Mathematical modelling and computing in biology and medicine*. Progetto Leonardo, Bologna.
- Chaloupka, M. 2001. Historical trends, seasonality and spatial synchrony in green sea turtle egg production. *Biological Conservation* 101:263–279.
- Chatfield, C. 1989. *The analysis of time series: an introduction*. 4th ed. Chapman & Hall, London.
- Climatic Research Unit. 2001. <http://www.cru.uea.ac.uk/cru/data/nao.htm>.
- Cook, E. R., D. M. Meko, and C. W. Stockton. 1997. A

- new assessment of possible solar and lunar forcing of the bidecadal drought rhythm in the Western United States. *Journal of Climate* 10:1343–1356.
- Crowley, T. J. 2000. Causes of climate change over the past 1000 years. *Science* 289:270–277.
- Currie, R. G. 1993a. Deterministic signals in European fish catches, wine harvest, and sea-level, and further experiments. *International Journal of Climatology* 13:665–687.
- . 1993b. Luni-solar 18.6 and 10–11 year solar cycle signals in USA air temperature records. *International Journal of Climatology* 13:31–50.
- . 1994. Variance contribution of luni-solar and solar cycle signals in the St. Lawrence and Nile river records. *International Journal of Climatology* 14:843–852.
- Currie, R. G., and D. P. O'Brien. 1988. Periodic 18.6 year and cyclic 10 to 11 year signals in north-eastern United States precipitation data. *International Journal of Climatology* 8:255–281.
- . 1990. Deterministic signals in precipitation records from the American corn belt. *International Journal of Climatology* 10:179–189.
- Dale, M. R. T., and M. Mah. 1998. The use of wavelets for spatial pattern analysis in ecology. *Journal of Vegetation Science* 9:805–815.
- Danell, K., L. Ericson, and K. Jakobsson. 1981. A method for describing former fluctuations of voles. *Journal of Wildlife Management* 45:1018–1021.
- Danell, K., S. Erlinge, G. Hogstedt, D. Hasselquist, E.-B. Olofsson, T. Seldal, and M. Svensson. 1999. Tracking past and ongoing lemming cycles on Eurasian tundra. *Ambio* 28:225–229.
- Earle, R. D., and K. R. Kramm. 1980. Techniques for age determination in the Canadian porcupine. *Journal of Wildlife Management* 44:413–419.
- Efron, B., and R. J. Tibshirani. 1993. *An introduction to the bootstrap*. Chapman & Hall, New York.
- Elton, C. 1924. Periodic fluctuations in the numbers of animals: their causes and effects. *British Journal of Experimental Biology* 2:119–163.
- Elton, C., and M. Nicholson. 1942. The ten-year cycle in numbers of the lynx in Canada. *Journal of Animal Ecology* 11:215–244.
- Erlinge, S., K. Danell, P. Frodin, D. Hasselquist, P. Nilsson, E.-B. Olofsson, and M. Svensson. 1999. Asynchronous population dynamics of Siberian lemmings across the Palaearctic tundra. *Oecologia (Berlin)* 119:493–500.
- Forchhammer, M. C., T. H. Clutton-Brock, J. Lindstrom, and S. D. Albon. 2001. Climate and population density induce long-term cohort variation in a northern ungulate. *Journal of Animal Ecology* 70:721–729.
- Foukal, P. V. 1990. The variable sun. *Scientific American* 262:34–41.
- Friis-Christensen, E. 2000. Solar variability and climate, a summary. *Space Science Reviews* 94:411–421.
- Friis-Christensen, E., and K. Lassen. 1991. Length of the solar cycle: an indicator of solar activity closely associated with climate. *Science* 254:698–700.
- Grenfell, B. T., K. Wilson, B. F. Finkenstädt, T. N. Coulson, S. Murray, S. D. Albon, J. M. Pemberton, T. H. Clutton-Brock, and M. J. Crawley. 1998. Noise and determinism in synchronized sheep dynamics. *Nature* 394:674–677.
- Grenfell, B. T., O. N. Bjørnstad, and J. Kappey. 2001. Travelling waves and spatial hierarchies in measles epidemics. *Nature* 414:716–723.
- Haigh, J. D. 1996. The impact of solar variability on climate. *Science* 272:981–984.
- . 1999. Modelling the impact of solar variability on climate. *Journal of Atmospheric, Solar and Terrestrial Physics* 61:63–72.
- . 2000. Solar variability and climate. *Weather* 55:399–407.
- . 2001. Climate variability and the influence of the Sun. *Science* 294:2109–2111.
- Hodell, D. A., M. Brenner, J. H. Curtis, and T. Guilderson. 2001. Solar forcing of drought frequency in the Maya lowlands. *Science* 292:1367–1370.
- Holling, C. S., and C. R. Allen. 2002. Adaptive inference for distinguishing credible from incredible patterns in nature. *Ecosystems* 5:319–328.
- Hoyt, D. V., and K. H. Schatten. 1997. *The role of the sun in climate change*. Oxford University Press, New York.
- Hudson, P. J., and I. M. Cattadori. 1999. The Moran effect: a cause of population synchrony. *Trends in Ecology & Evolution* 14:1–2.
- Hurrell, J. W. 1995. Decadal trends in the North Atlantic Oscillation: relationships to regional temperatures and precipitation. *Science* 269:676–679.
- Jaksic, F. M. 2001. Ecological effects of El Niño in terrestrial ecosystems of western South America. *Ecography* 24:241–250.
- Keith, L. B., and J. R. Cary. 1991. Mustelid, squirrel, and porcupine population trends during a snowshoe hare cycle. *Journal of Mammalogy* 72:373–378.
- Kerr, R. A. 1987. Sunspot-weather correlation found. *Science* 238:479–480.
- . 1988. Sunspot-weather link holding up. *Science* 243:1124–1125.
- . 1990. Sunspot-weather link is down but not out. *Science* 248:684–685.
- Krebs, C. J., R. Boonstra, S. Boutin, and A. R. E. Sinclair. 2001. What drives the 10-year cycle of snowshoe hares? *BioScience* 51:25–35.
- Langvatn, R., S. D. Albon, T. Burkey, and T. H. Clutton-Brock. 1996. Climate, plant phenology and variation in

- age of first reproduction in a temperate herbivore. *Journal of Animal Ecology* 65:653–670.
- Lean, J. L., J. Beer, and R. Bradely. 1995. Reconstruction of solar irradiance since 1610: implications for climate change. *Geophysical Research Letters* 22:3195–3198.
- Liebhold, A., and N. Kamata. 2000. Are population cycles and spacial synchrony a universal characteristic of forest insect populations? *Population Ecology* 42:205–209.
- Lima, M., J. E. Keymer, and F. M. Jaksic. 1999. El Niño–Southern Oscillation–driven rainfall variability and delayed density dependence cause rodent outbreaks in western South America: linking demography and population dynamics. *American Naturalist* 153:476–491.
- Lindstrom, J., H. Kokko, and E. Ranta. 1996. There is nothing new under the sunspots. *Oikos* 77:565–568.
- Loison, R., and R. Langvatn. 1998. Short- and long-term effects of winter and spring weather on growth and survival of red deer in Norway. *Oecologia (Berlin)* 116:489–500.
- MacLulich, D. A. 1937. Fluctuations in the numbers of the varying hare (*Lepus americanus*). University of Toronto Studies, series no. 43. University of Toronto Press, Toronto.
- Mallat, S. 1998. A wavelet tour of signal processing. Academic Press, San Diego, Calif.
- Mann, M. E., R. S. Bradley, and M. K. Hughes. 1998. Global-scale temperature patterns and climate forcing over the past six centuries. *Nature* 392:779–787.
- Meteorological Service of Canada. 2000. Canadian daily climate data: temperature and precipitation, Quebec. CD-ROM. Environment Canada, Downsview, Ontario.
- Mitchell, J. M., C. W. Stockton, and D. M. Mekko. 1979. Evidence of a 22-year rhythm of drought in the western United States related to the half solar cycle since the 17th century. Pages 125–143 in B. M. McCormac and T. A. Seliga, eds. *Solar terrestrial influences on weather and climate*. Reidel, Dordrecht.
- Moran, P. A. P. 1949. The statistical analysis of the sunspot and lynx cycles. *Journal of Animal Ecology* 18:115–116.
- . 1953a. The statistical analysis of the Canadian lynx cycle. I. Structure and prediction. *Australian Journal of Zoology* 1:163–173.
- . 1953b. The statistical analysis of the Canadian lynx cycle. II. Synchronization and meteorology. *Australian Journal of Zoology* 1:291–298.
- Morneau, C., and S. Payette. 1998. A dendroecological method to evaluate past caribou (*Rangifer tarandus* L.) activity. *Ecoscience* 5:64–76.
- . 2000. Long-term fluctuations of a caribou population revealed by tree-ring data. *Canadian Journal of Zoology* 78:1784–1790.
- Mursula, K., I. G. Usoskin, and G. A. Kovaltsov. 2001. Persistent 22-year cycle in sunspot activity: evidence for a solar magnetic field. *Solar Physics* 198:51–56.
- Myers, J. H. 1998. Synchrony in outbreaks of forest Lepidoptera: a possible example of the Moran effect. *Ecology* 79:1111–1117.
- Ottersen, G., B. Planque, A. Belgrano, E. Post, P. C. Reid, and N. C. Stenseth. 2001. Ecological effects of the North Atlantic Oscillation. *Oecologia (Berlin)* 128:1–14.
- Park, Y. H., and L. Gambéroni. 1995. Large-scale circulation and its variability in the south Indian Ocean from TOPEX/POSEIDON altimetry. *Journal of Geophysical Research* 100:24911–24929.
- Parker, K. L., C. T. Robbins, and T. A. Hanley. 1984. Energy expenditures for locomotion by mule deer and elk. *Journal of Wildlife Management* 48:474–488.
- Payette, S. 1987. Recent porcupine expansion at the tree line: a dendrochronological analysis. *Canadian Journal of Zoology* 65:551–557.
- Percival, D. 1995. On estimation of wavelet variance. *Biometrika* 82:619–631.
- Perry, C. A. 1994. Solar-irradiance variations and regional precipitation fluctuations in the western USA. *International Journal of Climatology* 14:969–983.
- Platt, J. R. 1964. Strong inference. *Science* 146:347–353.
- Post, E., and N. C. Stenseth. 1999. Climatic variability, plant phenology, and northern ungulates. *Ecology* 80:1322–1339.
- Post, E., N. C. Stenseth, R. Langvatn, and J. M. Fromentin. 1997. Global climate change and phenotypic variation among deer cohorts. *Proceedings of the Royal Society of London B* 264:1317–1324.
- Powell, R. A. 1982. *The fisher*. University of Minnesota Press, Minneapolis.
- Predavec, M., C. J. Krebs, K. Danell, and R. Hyndman. 2001. Cycles and synchrony in the collared lemming (*Dicrostonyx groenlandicus*) in Arctic North America. *Oecologia (Berlin)* 126:216–224.
- Ranta, E., V. Kaitala, J. Lindstrom, and E. Helle. 1997a. The Moran effect and synchrony in population dynamics. *Oikos* 78:136–142.
- Ranta, E., J. Lindstrom, V. Kaitala, H. Kokko, H. Linden, and E. Helle. 1997b. Solar activity and hare dynamics: a cross-continental comparison. *American Naturalist* 149:765–775.
- Reid, G. C. 2000. Solar variability and the earth's climate: introduction and overview. *Space Science Reviews* 94:1–11.
- Rind, D. 2002. The sun's role in climate variations. *Science* 296:673–677.
- Royama, T. 1992. *Analytical population dynamics*. Chapman & Hall, London.
- Roze, U. 1989. *The North American porcupine*. Smithsonian Institution, Washington, D.C.

- Ruohomäki, K., M. Tanhuanpää, M. P. Ayres, P. Kaitaniemi, T. Tammaru, and E. Haukioja. 2000. Causes of cyclicity of *Epirrita autumnata* (Lepidoptera, Geometridae): grandiose theory and tedious practice. *Population Ecology* 42:211–223.
- Saether, B. E. 1997. Environmental stochasticity and population dynamics of large herbivores: a search for mechanisms. *Trends in Ecology & Evolution* 12:143–149.
- Shindell, D., D. Rind, N. Balachandran, J. Lean, and P. Lonergan. 1999. Solar cycle variability, ozone, and climate. *Science* 284:305–308.
- Sinclair, A. R. E., and J. M. Gosline. 1997. Solar activity and mammal cycles in the Northern Hemisphere. *American Naturalist* 149:776–784.
- Sinclair, A. R. E., J. M. Gosline, G. Holdsworth, C. J. Krebs, S. Boutin, J. N. M. Smith, R. Boonstra, and M. Dale. 1993. Can the solar cycle and climate synchronize the snowshoe hare cycle in Canada? evidence from the tree rings and ice cores. *American Naturalist* 141:173–198.
- Smith, C. H. 1983. Spatial trends in Canadian snowshoe hare, *Lepus americanus*, populations cycles. *Canadian Field-Naturalist* 97:151–160.
- Spencer, D. A. 1964. Porcupine population fluctuations in past centuries revealed by dendrochronology. *Journal of Applied Ecology* 1:127–149.
- Stenseth, N. C., K. S. Chan, H. Tong, R. Boonstra, S. Boutin, C. J. Krebs, E. Post, et al. 1999. Common dynamic structure of Canada lynx population within three climatic regions. *Science* 285:1071–1073.
- Stenseth, N. C., A. Myrsetrud, G. Ottersen, J. W. Hurrell, K.-S. Chan, and M. Lima. 2002. Ecological effects of climate fluctuations. *Science* 297:1292–1296.
- Stockton, C. W., J. M. Mitchell, and D. M. Mekko. 1983. A reappraisal of the 22-year drought cycle. Pages 507–516 in B. M. McCormac, ed. *Weather and climate responses to solar variations*. Colorado Associated University Press, Boulder.
- Storini, M., and J. Sykora. 1997. Coronal activity during the 22-year solar magnetic cycle. *Solar Physics* 176:417–430.
- Sweitzer, R. A., and J. Berger. 1993. Seasonal dynamics of mass and body condition in Great Basin porcupines (*Erethizon dorsatum*). *Journal of Mammalogy* 74:198–203.
- Torrence, C., and G. P. Compo. 1998. A practical guide to wavelet analysis. *Bulletin of the American Meteorological Society* 79:61–78.
- Udelhofen, P. M., and R. D. Cess. 2001. Cloud cover variations over the United States: an influence of cosmic rays or solar variability. *Geophysical Research Letters* 28:2617–2620.
- van Loon, H., and K. Labitzke. 1988. Association between the 11-year solar cycle, the QBO, and the atmosphere. II. Surface and 700 mb on the northern hemisphere in winter. *Journal of Climate* 1:905–920.
- . 1998. The global range of the stratospheric decadal wave. I. Its association with the sunspot cycle in summer and in the annual mean, and with the troposphere. *Journal of Climate* 11:1529–1537.
- . 2000. The influence of the 11-year solar cycle on the stratosphere below 30 km: a review. *Space Science Reviews* 94:259–278.
- Vautard, R., P. Yiou, and M. Ghil. 1992. Singular spectrum analysis: a toolkit for short, noisy chaotic signals. *Physica D* 58:95–126.
- Verschuren, D., K. R. Laird, and B. F. Cumming. 2000. Rainfall and drought in equatorial east Africa during the past 1,100 years. *Nature* 403:410–414.
- Weladji, R. B., and Ø. Holand. 2003. Global climate change and reindeer: effects of winter weather on the autumn weight and growth of calves. *Oecologia (Berlin)* 136:317–323.
- White, L., and F. Johns. 1997. Marine environmental assessment of the estuary and gulf of St. Lawrence. Fisheries and Oceans Canada, Dartmouth, Nova Scotia, and Mont-Joli, Quebec.
- White, W. B., J. Lean, D. R. Cayan, and M. D. Dettinger. 1997. Response of global upper ocean temperature to changing solar irradiance. *Journal of Geophysical Research* 102:3255–3266.
- World Data Centre for the Sunspot Index. 2001. <http://sidc.oma.be/html/sunspot.html>.

Appendix A from I. Klvana et al., “Porcupine Feeding Scars and Climatic Data Show Ecosystem Effects of the Solar Cycle” (Am. Nat., vol. 164, no. 3, p. 283)

Scar Sampling and Dating

Technical Details on Scar Sampling

Stand 1 (48°21'30"N, 68°48'30"W) had an area of 14 ha and was even aged, composed mostly of 117-year-old jack pine, although some trees were up to 150 years old and had porcupine feeding scars up to 133 years old. Scars were sampled within 29 circular 400-m² plots located at 25-m intervals along a transect running through the entire jack pine stand. Within the plots, all jack pines were inspected for presence of scars, and all scars found on the trunks between 0 and 1.8 m off the ground were cored ($n = 575$). Because the majority of scars were found near ground level, it is very unlikely that sampling only between 0 and 1.8 meters off the ground introduced a bias in our results. Of these, 501 scars located on 357 trees were dated with accuracy and used for analysis. Stand 2 (48°20'30"N, 68°49'30"W) had an area of 5 ha and was even aged, composed mostly of 105-year-old jack pine. Because of the relative scarcity of scars, all jack pines in stand 2 were inspected, and all scars found on the trunks between 0 and 1.8 m off the ground were cored ($n = 519$). Of these, 487 scars located on 369 trees were dated with accuracy and used for analysis. Stand 3 (48°15'30"N, 68°59'30"W) had an area of 2 ha and was also even aged, composed mostly of 77-year-old jack pine. All jack pines in the stand were inspected, and all scars found on the trunk between 0 and 1.8 m off the ground were cored ($n = 373$). Of these, 302 scars located on 206 trees were dated with accuracy and used for analysis.

Technical Details on Scar Dating

Cores were started in sound wood on the surface of a scar or at the edge of a scar and were taken across the entire diameter of the trunk. Because only live trees were sampled, the last growth ring located on the opposite side from the scar, together with diagnostic growth ring sequences, served as reference years for dating back to the scar. Two cores were taken per scar to ensure accurate dating. Cores were glued onto grooved plywood boards directly in the field, air dried, and finely sanded in the laboratory. Year of scar formation was determined under a binocular lens by counting tree rings. Because most scars in our study sites were produced in November and December (I. Klvana, unpublished data), all scars were dated as if they were produced at the end of a calendar year (November or December) in the same year as the preceding growing season. Reliability of coring as opposed to taking cross sections (Payette 1987) was verified by comparing dates obtained from cores and cross sections of 30 scars. When two or more scars of the same age were found on a given tree (5.3% of cases), only one of them was considered in a preliminary analysis. However, this decision did not affect the results, so we included all scars in our final analyses. Some authors considered temporal changes in the availability of trees (on the basis of age distribution of trees) when reconstructing past animal activity from tree ring data (Sinclair et al. 1993; Morneau and Payette 1998, 2000). We did not do so because the trees sampled were mostly even-aged jack pine.

Appendix B from I. Klvana et al., “Porcupine Feeding Scars and Climatic Data Show Ecosystem Effects of the Solar Cycle” (Am. Nat., vol. 164, no. 3, p. 283)

The Wavelet Analysis

Wavelets constitute a family of functions derived from a single function, the mother wavelet $\psi(t)$, which can be expressed as function of two parameters, one for the time position, τ , and the other for the scale of the wavelets, a , related to the frequency. More explicitly, wavelets are defined as

$$\psi_{a,\tau}(t) = \frac{1}{\sqrt{a}} \psi\left(\frac{t-\tau}{a}\right). \quad (\text{B1})$$

The wavelet transform of a time series $x(t)$ with respect to a chosen wavelet $\psi(a, \tau)$ is computed as the convolution between the wavelet and the signal $x(t)$:

$$W_x(a, \tau) = \frac{1}{\sqrt{a}} \int_{-\infty}^{+\infty} x(t) \psi^*\left(\frac{t-\tau}{a}\right) dt = \int_{-\infty}^{+\infty} x(t) \psi_{a,\tau}^*(t) dt, \quad (\text{B2})$$

with an asterisk indicating the complex conjugate form. The wavelet coefficients $W_x(a, \tau)$ represent the contribution of the scales, a , to the signal at different time positions, τ . The computation of the wavelet transform is done along the signal $x(t)$ (by increasing the τ parameter) over a range of a scales until all the coherent structures within the signal can be identified.

In the analysis of “natural signals,” the so-called Morlet wavelet (Torrence and Compo 1998) is often applied. The Morlet wavelet is defined as

$$\psi(t) = \pi^{-1/4} \exp(-i2\pi f_0 t) \exp\left(-\frac{t^2}{2}\right). \quad (\text{B3})$$

In our study, we have used $f_0 = 6$. An important point here is that a is inversely proportional to the central frequency of the wavelet f_0 . In fact, with the Morlet wavelet and the value used for f_0 , the frequency is equal to $1/a$, or the period, p , is equal to a ($f = 1/a$ or $p = a$).

As with classical Fourier analysis using Fast Fourier Transform, the data were padded with zeros up to the next-highest power of two (Torrence and Compo 1998). We defined the “cone of influence” to delineate a region near the start and the end of the series where there is a loss in statistical power and in which the values should be interpreted cautiously. Nevertheless, the zero padding, owing to numerous introduced zeros, mainly induces a reduction in the numerical values of the wavelet transform and their associated quantities.

In addition to the wavelet transform coefficients, we estimated the repartition of variance between a or p and different τ . This is known as the wavelet power spectrum, $S_x(p, \tau) = |W_x(p, \tau)|^2$. At each time considered, the result is a three-dimensional surface $W_x(a, \tau)$ or $S_x(p, \tau)$, and we presented a 2D plot (names scalogram) of these quantities against p and τ parameters.

We also time averaged the wavelet power spectrum to obtain a quantity analogous to the Fourier power spectrum (called here the global wavelet power spectrum):

$$\bar{S}_x(p) = \frac{\sigma_x^2}{T} \int_0^T |W_x(p, \tau)|^2 d\tau, \quad (\text{B4})$$

with σ_x^2 as the variance and T as the time duration of the time series $x(t)$. Percival (1995) has shown that the global wavelet power spectrum provides an unbiased and consistent estimation of the classical Fourier spectrum.

To quantify statistical relationships between two time series, we used wavelet coherence (Chatfield 1989). We computed these quantities using wavelet transform, and the wavelet coherence reads

$$R_{x,y}(p, \tau) = \frac{|\langle W_{x,y}(p, \tau) \rangle|^2}{|\langle W_x(p, \tau) \rangle|^2 |\langle W_y(p, \tau) \rangle|^2}, \quad (\text{B5})$$

where $\langle \cdot \rangle$ and $\langle \cdot \rangle$ indicate smoothing in both time and period, $W_x(p, \tau)$ is the wavelet transform of series $x(t)$, $W_y^*(p, \tau)$ is the wavelet transform of $y(t)$, and $W_{x,y}(p, \tau)$ is the cross-wavelet transform defined as $W_{x,y}(p, \tau) = W_x(p, \tau)W_y^*(p, \tau)$. The smoothing is performed as in traditional Fourier approaches by a convolution with a constant window function both in time and frequency directions (Chatfield 1989). The wavelet coherence, $R_{x,y}(p, \tau)$, provides local information about where two nonstationary signals, $x(t)$ and $y(t)$, are linearly correlated at a particular period. The coherence varies between 0 and 1. $R_{x,y}(p, \tau)$ is equal to 1 when there is a perfect linear relation at a particular time and period between two signals.

In complement to wavelet analysis, we used phase analysis to characterize and quantify the association between signals (Cazelles and Stone 2003). The phase difference provided information on the sign of the relationship (i.e., in phase or out of phase relations). Because the Morlet wavelet is a complex wavelet, we can write $W_x(p, \tau)$ in terms of its phase $\phi_x(p, \tau)$ and modulus $|W_x(p, \tau)|$. The phase of the Morlet transform varies cyclicly between $-\pi$ and π over the duration of the component waveforms and is defined as

$$\phi_x(p, \tau) = \tan^{-1} \frac{\Im(W_x(p, \tau))}{\Re(W_x(p, \tau))}. \quad (\text{B6})$$

We used resampling methods to quantify the statistical significance of the patterns exhibited by the wavelet approach (Cazelles and Stone 2003). We therefore constructed new data sets from the observed time series, which shared with the original signals some properties but were built under the null hypothesis that the variability of the observed time series or the association between two time series is not different to that expected by chance alone. The building of controlled data sets was performed by classical resampling methods (Efron and Tibshirani 1993). We computed the wavelet transform and other estimated quantities (e.g., wavelet power spectrum and coherence) for each bootstrapped time series, therefore generating the distribution of these quantities under the null hypothesis. To test whether the analyzed time series were inconsistent with the null hypothesis, we compared quantities obtained from these series with the distribution of quantities obtained from bootstrapped series. Then P values were obtained as a fraction of the control data sets giving estimated quantities that were larger than those obtained from the analyzed series.

This statistical approach was also applied to the phase analyses. We quantified the phase difference between two time series by the normalized entropy of their distributions (Cazelles and Stone 2003). This approach quantifies the association between the phases of two time series over the entire period, in contrast to the wavelet coherence that quantifies locally the phase association. In the case of nonstationary phase associations, the phase difference would be nonsignificant over the entire time period.

We performed all analyses using original algorithms developed in Matlab (version 6.5, MathWorks). These original algorithms incorporate both cross analyses and adapted statistical procedures (B. Cazelles, M. Chavez, D. Berteaux, F. Ménard, J. Vik, S. Jenouvrier, and N. Stenseth, unpublished manuscript).

**Appendix C from I. Klvana et al., “Porcupine Feeding Scars and Climatic Data Show Ecosystem Effects of the Solar Cycle”
(Am. Nat., vol. 164, no. 3, p. 283)**

Literature Review on the Link between the Solar Cycle and Climate

There is growing evidence that variations in solar activity have effects on the earth’s climate at several timescales. However, much about these effects remains to be understood (Rind 2002). Evidence of a solar activity–climate link appears strongest at the timescale of centuries and millennia, as suggested by both region-specific (Verschuren et al. 2000; Bond et al. 2001; Hodell et al. 2001) and planetwide studies (Mann et al. 1998; Crowley 2000). These long-term solar-related climatic oscillations have even been shown to affect human cultural development, in both Africa (Verschuren et al. 2000) and America (Hodell et al. 2001), suggesting a cascading effect of variations in solar activity on entire ecosystems.

There is also much evidence of a solar activity–climate link at the timescale of the 11-year and 22-year solar cycles. The 11-year solar cycle signal was detected in various climatic and climate-related data, such as U.S. precipitation and temperature records, St. Lawrence and Nile river flows, European fish catches, wine harvests, and sea levels (Currie and O’Brien 1988, 1990; Currie 1993*a*, 1993*b*, 1994). Perry (1994) found that precipitation fluctuations in certain regions of the United States were highly correlated with solar activity in previous years, while in other regions the correlation was weak or absent. This same periodicity in precipitation was detected in net snow accumulation data from a glacier in the Yukon (Sinclair et al. 1993). Variations in cloud cover over the United States were also found to be related to the solar cycle (Udelhofen and Cess 2001). The 22-year Hale solar cycle was shown to play a role in the timing and extent of drought in the United States (Mitchell et al. 1979; Stockton et al. 1983; Cook et al. 1997).

In addition to climatic responses to the solar cycle at the regional and continental scale, global planetwide responses have also been observed. White et al. (1997) and Reid (2000) have shown that changes in solar irradiance at the scale of both the 11-year and 22-year solar cycles are reflected in the surface sea temperatures across the Pacific, Atlantic, and Indian Oceans. But it is perhaps the correlation found by van Loon and Labitzke (1988, 1998, 2000) between the solar cycle and the temperatures and heights of the stratosphere at 30 hPa and below that is the most well-known and striking evidence of a solar cycle–climate link (Kerr 1987, 1988, 1990; Haigh 2000, 2001). Modeling studies of the earth’s climate (Haigh 1996, 1999; Shindell et al. 1999) corroborate some of the empirical evidence of a solar cycle–climate link. However, in many cases, the observed climatic response is much greater than what can be expected on the basis of the fact that solar irradiance varies by only 0.1% from the minimum to the maximum of an 11-year cycle. This raises questions about the underlying physical mechanisms and suggests the existence of amplifying mechanisms (Friis-Christensen and Lassen 1991; Friis-Christensen 2000; Haigh 2000; Rind 2002). Also, the effect of the solar cycle is not felt in the same way and with the same intensity in different regions of our planet, and our limited knowledge of our planet’s climate does not allow us to understand these regional discrepancies (Hoyt and Schatten 1997; Rind 2002).

**Appendix D from I. Klvana et al., “Porcupine Feeding Scars and Climatic Data Show Ecosystem Effects of the Solar Cycle”
(Am. Nat., vol. 164, no. 3, p. 283)**

Online Figures

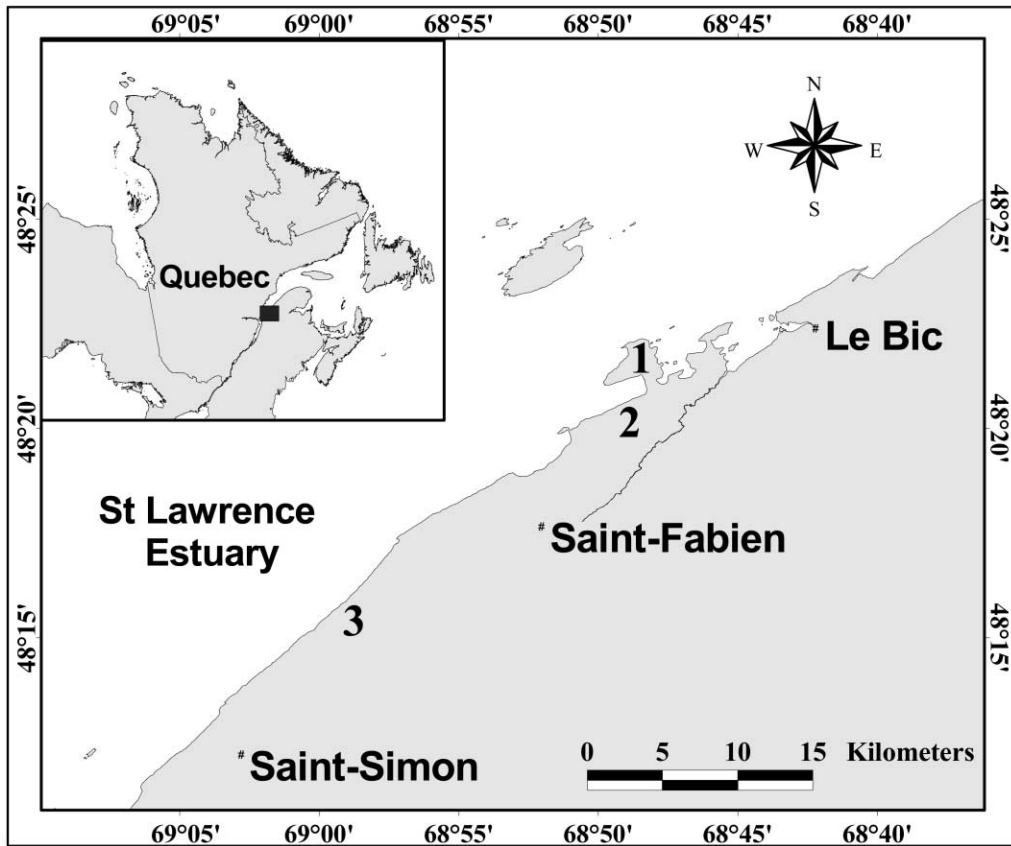
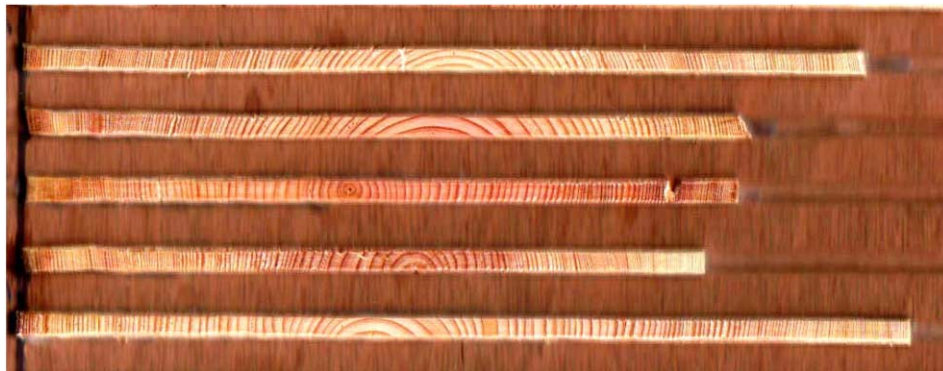


Figure D1: Map showing the location of the three jack pine stands (labeled 1, 2, and 3) in which porcupine feeding scars were sampled.



Figure D2: Photograph of a jack pine trunk showing a porcupine scar being cored



Scar end

live end

Figure D3: Photograph of mounted cores used for dating of porcupine feeding scars. The scar ends are on the left side, and the live ends are on the right side. The age of a scar is obtained by subtracting the number of rings between the center of the tree and the scar from the number of rings between the center of the tree and the year of sampling.

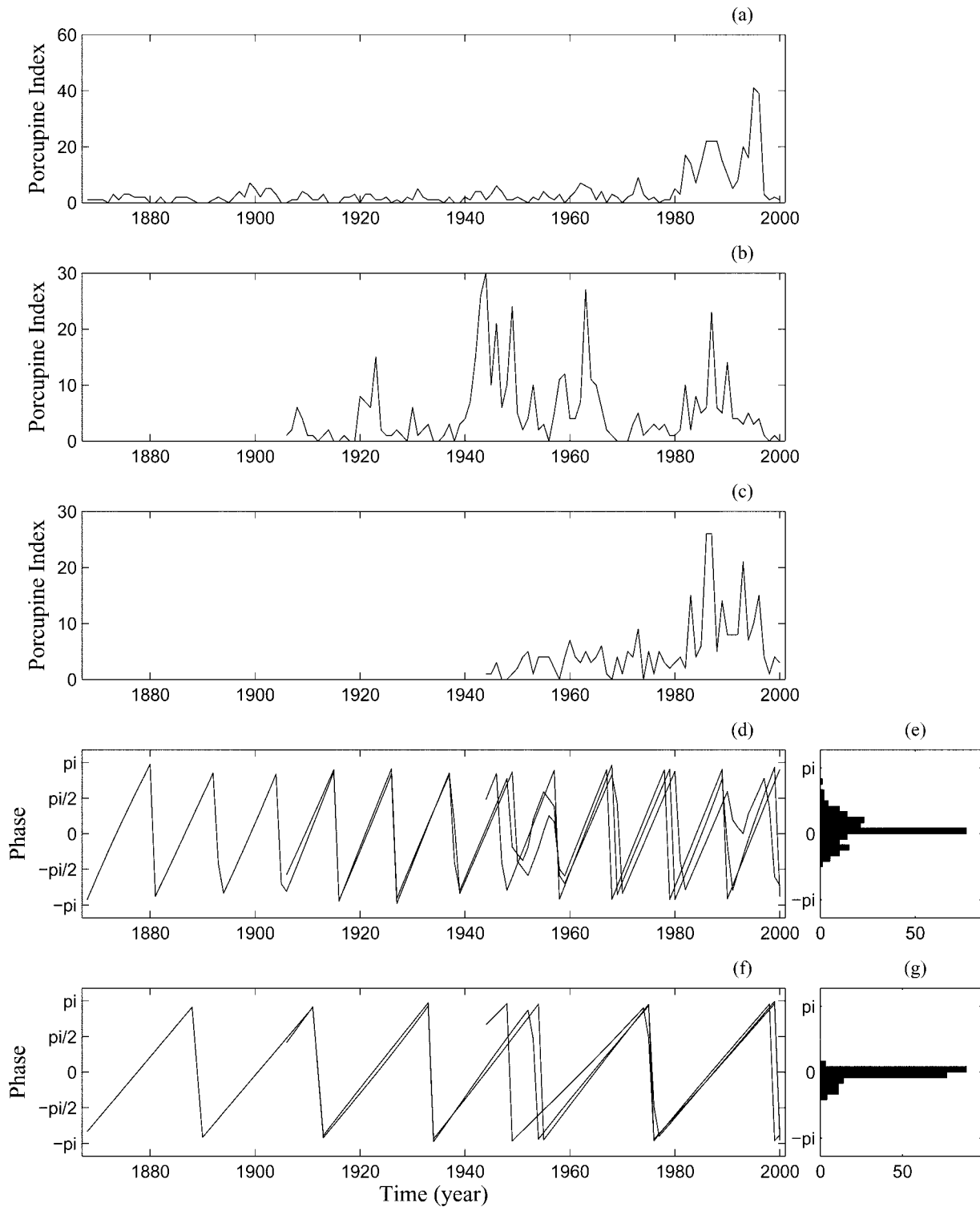


Figure D4: Frequency distribution of the number of porcupine feeding scars at three study sites in the Lower St. Lawrence region of eastern Quebec, Canada. *a*, Site 1. *b*, Site 2. *c*, Site 3 (see app. A for details about scar sampling at each site). *d*, Phase time series of porcupine abundance index in each of the three study sites,

App. D from I. Klvana et al., “Solar Cycle and Porcupine Fluctuations”

computed in the 10–12-year periodic band. *e*, Distribution of phase differences; normalized entropy of the distribution (pairwise comparisons) = 0.38, $P = .002$ based on 500 bootstrapped series. *f*, *g*, Same as *d*, *e*, but computed in the 21–23 periodic band; normalized entropy of the distribution (pairwise comparisons) = 0.48, $P = .004$ based on 500 bootstrapped series.

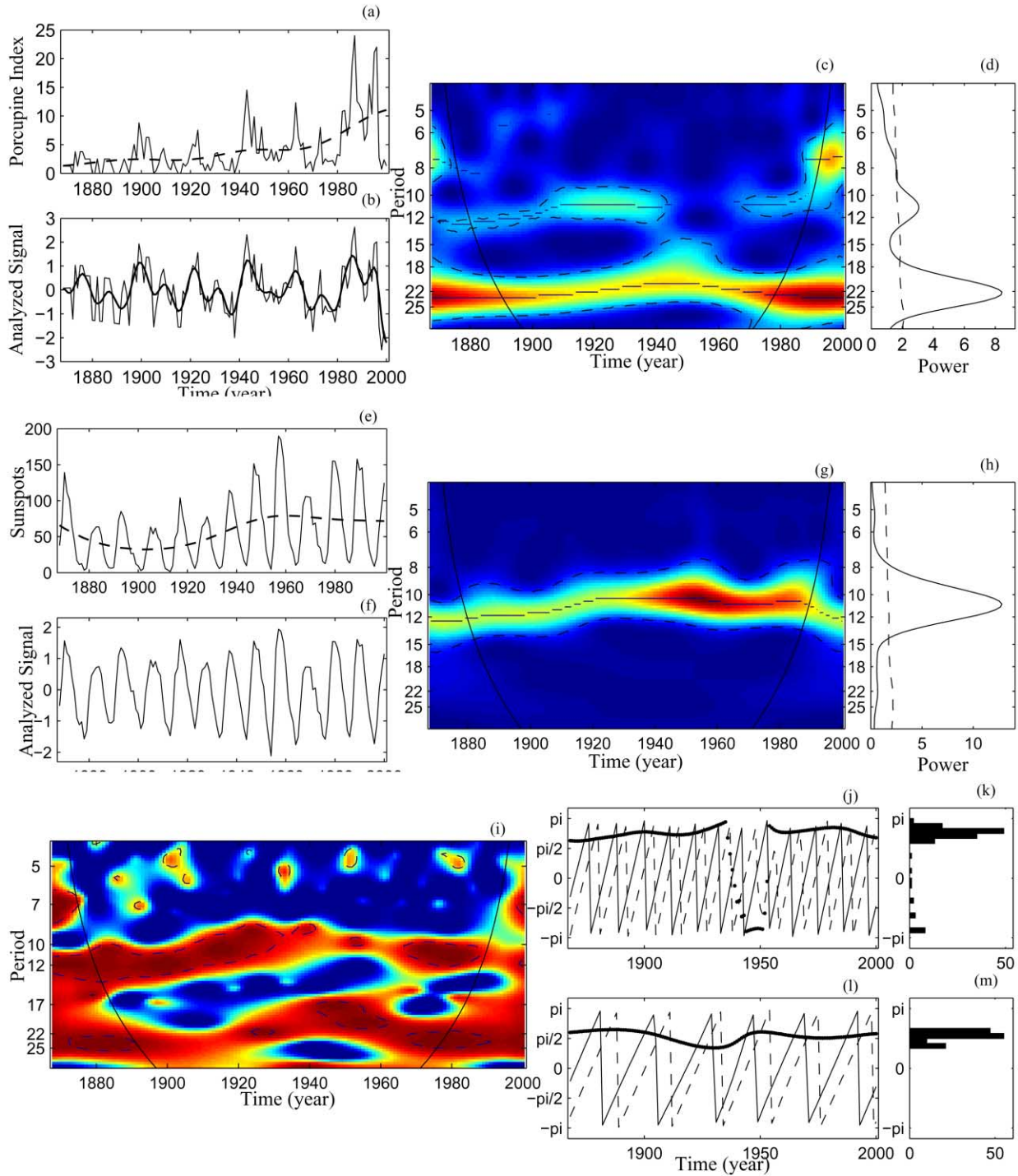


Figure D5: Wavelet analysis of porcupine abundance index and sunspot number. *a*, Porcupine abundance index (*solid line*) calculated as the pooled frequency distribution of porcupine feeding scars from three sites in eastern Quebec, Canada. The dashed line shows high-period (>50 years) oscillating components. *b*, Analyzed time series (*thin line*) obtained by square root transformation of *a*, followed by detrending through the subtraction of high-period oscillating components. To underline the periodic components in the data, a smoothed series, obtained using Singular Spectrum Analysis (Vautard et al. 1992), is also shown (*bold line*); this last series was not used in

the analysis. *c*, Local wavelet power spectrum (i.e., scalogram) of *b*. Low power values are represented in dark blue and high power values in dark red. The black dashed lines show the $\alpha = 5\%$ significance level computed based on 500 bootstrapped series. The crests of the oscillations and the cone of influence, which indicate the region not influenced by edge effects, are also shown on the scalogram. *d*, Global wavelet power spectrum (similar to the classical Fourier spectrum) of *b*. The dashed line shows the $\alpha = 5\%$ significance level computed based on 500 bootstrapped series. *e*, Sunspot number (*solid line*). The dashed line shows high-period (>50 years) oscillating components. *f*, Analyzed time series (*thin line*) obtained by square root transformation of *a*, followed by detrending through the subtraction of high-period oscillating components. *g*, Local wavelet power spectrum (i.e., scalogram) of *f*. Interpretation similar to scalogram *c*. *h*, Global wavelet power spectrum of *f*. The dashed line shows the $\alpha = 5\%$ significance level computed based on 500 bootstrapped series. *i*, Coherence between sunspot number and porcupine abundance index; interpretation similar to scalogram *c*. *j*, Phase time series of sunspot number (*thin solid line*) and porcupine abundance index (*dashed line*) computed in the 10–12-year periodic band. The bold line displays the phase difference evolution. *k*, Distribution of phase differences; normalized entropy of the distribution = 0.45, $P = .008$ based on 500 bootstrapped series. *l*, Same as *j* but computed in the 21–23 periodic band. *m*, Distribution of phase differences; normalized entropy of the distribution = 0.42, $P = .016$ based on 500 bootstrapped series.

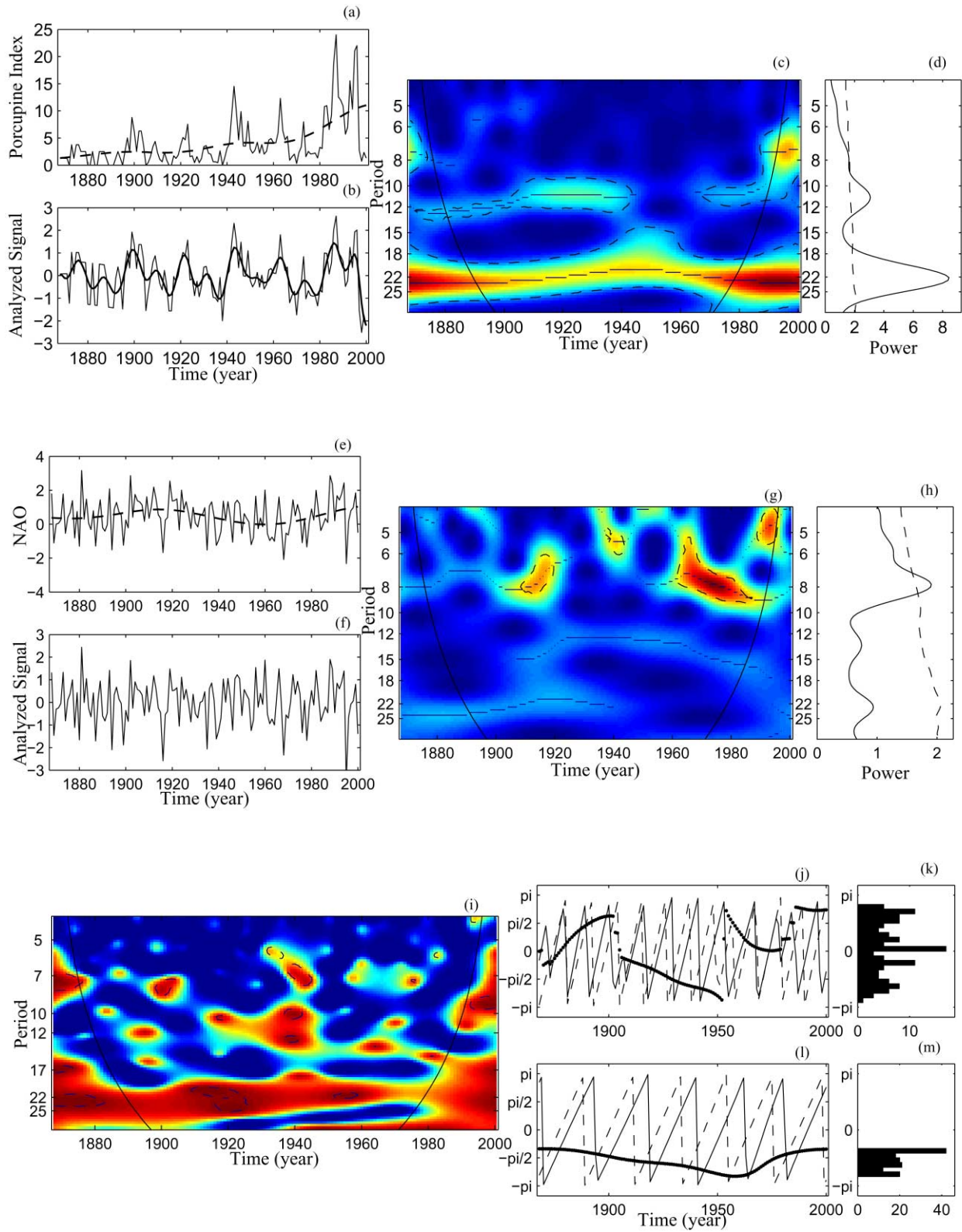


Figure D6: Wavelet analysis of porcupine abundance index and winter NAO index. *a*, Porcupine abundance

index (*solid line*) calculated as the pooled frequency distribution of porcupine feeding scars from three sites in eastern Quebec, Canada. The dashed line shows high-period (>50 years) oscillating components. *b*, Analyzed time series (*thin line*) obtained by square root transformation of *a*, followed by detrending through the subtraction of high-period oscillating components. To underline the periodic components in the data, a smoothed series, obtained using Singular Spectrum Analysis (Vautard et al. 1992), is also shown (*bold line*); this last series was not used in the analysis. *c*, Local wavelet power spectrum (i.e., scalogram) of *b*. Low power values are represented in dark blue and high power values in dark red. The black dashed lines show the $\alpha = 5\%$ significance level computed based on 500 bootstrapped series. The crests of the oscillations and the cone of influence, which indicate the region not influenced by edge effects, are also shown on the scalogram. *d*, Global wavelet power spectrum (similar to the classical Fourier spectrum) of *b*. The dashed line shows the $\alpha = 5\%$ significance level computed based on 500 bootstrapped series. *e*, Winter NAO index (*solid line*). The dashed line shows high-period (>50 years) oscillating components. *f*, Analyzed time series (*thin line*) obtained by square root transformation of *a*, followed by detrending through the subtraction of high-period oscillating components. *g*, Local wavelet power spectrum (i.e., scalogram) of *f*. Interpretation similar to scalogram *c*. *h*, Global wavelet power spectrum of *f*. The dashed line shows the $\alpha = 5\%$ significance level computed based on 500 bootstrapped series. *i*, Coherence between winter NAO index and porcupine abundance index; interpretation similar to scalograms *c* and *g*. *j*, Phase time series of winter NAO index (*thin solid line*) and porcupine abundance index (*dashed line*) computed in the 10–12-year periodic band. The bold line displays the phase difference evolution. *k*, Distribution of phase differences; normalized entropy of the distribution = 0.08, $P > .1$ based on 500 bootstrapped series. *l*, Same as *j* but computed in the 21–23 periodic band. *m*, Distribution of phase differences; normalized entropy of the distribution = 0.36, $P > .1$ based on 500 bootstrapped series.